

*Article*

## SCAPS Numerical Analysis of Solid-State Dye-Sensitized Solar Cell Utilizing Copper (I) Iodide as Hole Transport Layer

Nur Syamimi Nooraid<sup>1,a</sup>, Faiz Arith<sup>1,b,\*</sup>, Ain Yasmin Firhat<sup>1,c</sup>,  
Ahmad Nizamuddin Mustafa<sup>2,d</sup>, and Ahmad Syahiman Mohd Shah<sup>3,e</sup>

<sup>1</sup> Centre for Telecommunication Research & Innovation, Faculty of Electronic and Computer Engineering, Universiti Teknikal Malaysia Melaka, Hang Tuah Jaya, 76100, Durian Tunggal, Malaysia

<sup>2</sup> Centre for Telecommunication Research & Innovation, Faculty of Electrical and Electronic Engineering Technology, Universiti Teknikal Malaysia Melaka, Hang Tuah Jaya, 76100, Durian Tunggal, Malaysia

<sup>3</sup> Department of Electrical Engineering, College of Engineering, Universiti Malaysia Pahang, Lebuhraya Tun Razak, 26300 Gambang, Kuantan, Pahang, Malaysia

E-mail: <sup>a</sup>nursyamiminooraid@yahoo.com, <sup>b,\*</sup>faiz.arith@utem.edu.my (Corresponding author),  
<sup>c</sup>ain.yasmin.firhat@gmail.com, <sup>d</sup>nizamuddin@utem.edu.my, <sup>e</sup>asyahiman@ump.edu.my

**Abstract.** Here, numerical study of solid-state dye-sensitized solar cell (SSDSSC) with Copper (I) Iodide as a hole transport layer was investigated using SCAPS-1D simulation software. The complete simulated device structures in this project are composed of FTO/TiO<sub>2</sub>/N719/CuI/Ni. Several key parameters of HTL such as layer thickness, doping concentration, working temperature, and interface defect have been analysed to obtain the highest efficiency for SSDSSC as well as the influence of back contact. The incorporation with various ETLs such as TiO<sub>2</sub>, ZnO, and SnO<sub>2</sub> were also studied. The results show that SSDSSC with back contact yields a better performance due to low HTL thickness compared to without back contact. In addition, it can also be proved that TiO<sub>2</sub> as ETL obtained the best efficiency up to 5.6%. Further investigation also found that combining optimized CuI and TiO<sub>2</sub> parameters with a perovskite layer would increase cell efficiency to nearly 30%, higher than previously reported devices. The proposed parameter structure may trigger the temptation for the use of CuI as HTL in solar cell application.

**Keywords:** CuI, hole transport layer, SCAPS-1D, SSDSSC, perovskite solar cell.

ENGINEERING JOURNAL Volume 26 Issue 2

Received 26 August 2021

Accepted 4 February 2022

Published 28 February 2022

Online at <https://engj.org/>

DOI:10.4186/ej.2022.26.2.1

## 1. Introduction

In recent years, global energy demand has continued to increase dramatically with about 80% to 85% of the energy used being produced by fossil fuels. Solar energy is one of the candidates that can replace this non-renewable energy source and at the same time balance the energy needs of humans [1, 2]. Solar energy is naturally replenished on a human timescale and is always readily available [3]. Generally, a solar cell is a device that produces electrical energy from the direct conversion of sunlight through the photovoltaic effect [4, 5]. Over the years, the solar cell has gone through a few revolutions resulting in a three-generation of solar cell. The third generation of solar cells is a promising emerging new technology, expected to meet the needs of human energy in the future. This generation aims for better cell efficiency at low cost, where simple fabrication technology and low production costs. At present, the most growing solar cells are Solid-State Dye-Sensitized Solar Cell (SSDSSC) [6].

SSDSSC is a photochemical cell that produces electrical energy when dye immobilized becomes excited onto an all-solid structure cell. This is an alternative to overcoming the former Dye-Sensitized Solar Cell (DSSC) which implements liquid electrolyte in its mechanism, where it suffers from leakage and corrosive nature issues [7, 8]. Quasi solid-state or solid hole conductors have been introduced to address the issue of liquid electrolytes [9]. Basically, the SSDSSC is composed of five basic structures including front contact, Electron Transport Layer (ETL), dye-sensitizer, Hole Transport Layer (HTL), and back contact. The parameter for each layer structure contribute a massive impact on the performance of SSDSSC [10, 11].

CuI is a p-type semiconductor material, used in solar cells as an HTL. CuI has become an attraction among researchers due to its promising features such as small resistivity with the order of  $10^{-2} \Omega\text{-cm}$ , photosensitivity, huge temperature dependency, negative spin-orbit splitting, high optical absorption, large bandgap, considerable exciton binding and high mobility [12, 13]. CuI offers three main properties as a promising HTL: (1) facilitate charge transportation with a matching HOMO and LUMO level of HTL with HOMO level of dye and conduction band of  $\text{TiO}_2$  [4] (2) high hole mobility [12] (3) amorphous, which can be deposit within porous  $\text{TiO}_2$  layer [14, 15].

In addition, CuI is a viable alternative to organic HTL due to its increased efficiency and stability over other HTL materials [16]. This is principally due to high hole conductivity and valence band maximum properties, which is well-aligned with the absorbent layer. Previous research has shown that replacing organic HTL with CuI leads to enhanced efficiency and stability due to reduced cell hysteresis, improved charge extraction, and prevented charge recombination. Furthermore, as the aging period of CuI is extended, the PSC efficiency

increases due to the reduction of energy loss at the HTL/perovskite interface leads to an improve interface contact. Moreover, using encapsulated CuI as HTL has improved air stability.

F. Jahantigh *et al.* (2019) [9] have reported the first and only study on numerical simulation analysis of HTL materials in SSDSSC. The effects of different organic and inorganic materials of Spiro-OMeTAD, PEDOT: PSS, CuSCN and CuI on cell performance were investigated. As a result, they claimed that inorganic CuI HTL is the best by producing Power Conversion Efficiency (PCE) as high as 17.72%. This work has been the impetus for the use of CuI as HTM in improving the efficiency and stability of devices. However, the results obtained rather interesting yet questionable.

S.Prabath *et al.* simulated and compared the efficiency between conventional HTM(Spiro-Ometad) and PEDOT:PSS HTM. It claimed that the use of Spiro-Ometad as HTL has resulted in a higher efficiency of 12.13% compared to PEDOT: PSS which was merely 11.89% [17]. Jiasing *et al.* has fabricated PSCs utilizing PEDOT:PSS, which was integrated with Au nanochains plasmonic nanostructure as HTL. The highest cell efficiency obtained in this work was 19.2%, mainly contributed by the enhanced electrical characteristics, increased optical absorption and exhibiting a significant increase in stability [18]. Emily *et al.* claimed that the use of DMF as a solvent changes the electrical conductivity of CuI, which can improve charge extraction in complete photovoltaic devices. Besides, it also proved that the active layer fabrication process has an effect on the HTL profile, where CuI is utilized as a hole transport material in p-i-n perovskite solar cells[16].

CuI has also been extensively studied as HTL in other types of solar cells. Y. Gan *et al.* (2020) [19] have reported PCE of 17.79% by incorporation the CuI HTL in Perovskite Solar Cell (PSC). Although it is widely known that the PCE for PSC is supposed to be better, but the results obtained are almost similar than that in previous SSDSSC report [12]. This deficiency is most probably due to the band alignment where the valence band level of CuI is higher than the absorber layer, forming an energy cliff at the perovskite/HTL interface. Therefore, this increases the possibility of interface recombination and results in a reduction of the current generated.

Organic Solar Cells (OSC) also encounter similar problems with HTL materials, where the conventional HTL PEDOT: PSS suffers from uncertainty in its electron blocking ability and acidic nature state [20]. K. S. Nithya *et al.* (2020) [21] has reported a simulated device modelling of a Non-Fullerene Organic Solar Cell (NFA-OSC) utilizing CuI as HTL, resulting in an optimum PCE of 15.68%. Several key parameters: active layer thickness, defect density of the active layer and at interface layer, HTL and ETL properties were varied to obtain the finest cell performance.

This work proposed CuI as an alternative HTL of OSC, due to increased PCE as well as cell stability.

Herein, we have extensively studied the effect of CuI as HTL material in SSDSSC upon several parameter. Cell efficiency as high as 5.6% was obtained with HTL layer thickness of 2.2  $\mu\text{m}$ . This layer is thicker than the previous simulated report, thus accelerates the fabrication process and the cost for cell production become more effective. The effect of the presence of back contact on SSDSSC performance and different absorbance layer were also studied. Thus, our work results show that SSDSSC utilizing CuI as HTL with Ni as back contact is promising in cell efficiency improvement.

## 2. Device Simulation

In this work, SSDSSC utilizing CuI as HTL was simulated using SCAPS-1D 3.8 version 2020 software [22]. The device structure of SSDSSC is composed of 5 main layers: FTO as front contact,  $\text{TiO}_2$  as ETL, N719 as dye-sensitizer, CuI as HTL, and Ni as back contact as shown in Fig. 1. Figure 2 shows the band alignment of simulated device structure of SSDSSC. There are a few parameters that were analysed to obtain the optimum cell efficiency of SSDSSC based on the factor of the presence of Ni as a back contact and incorporation of different ETL materials. The layer thickness, doping density of CuI, device working temperature, back contact, front contact, and the interface defect on each layer were varied and studied thoroughly. The sunlight is set under default illumination of AM1.5G, 100  $\text{MW}\cdot\text{cm}^{-2}$  in SCAPS-1D simulation. The general SCAPS input and fundamental parameters of each component are as demonstrated in Table 1.

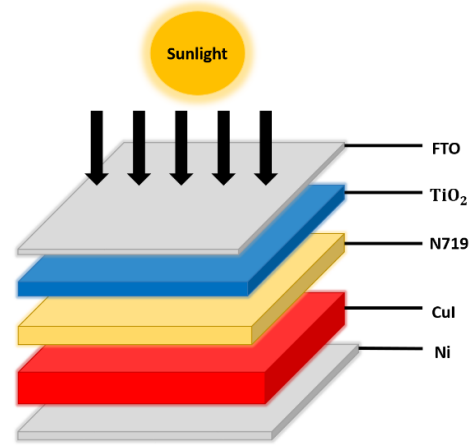


Fig. 1. The simulated device structure of SSDSSC.

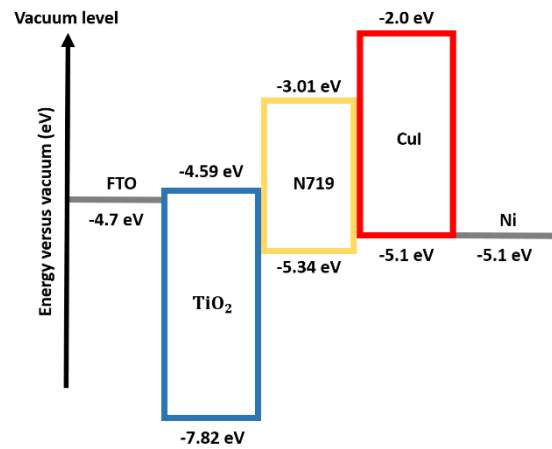


Fig. 2. Band alignment (relative to vacuum level) of simulated device structure of SSDSSC [38–40].

Table 1. Parameters of the component in device modelling of SSDSSC.

Parameter	CuI [9]	N719 [9]	$\text{TiO}_2$ [9]	FTO [23]	ZnO [23]	$\text{SnO}_2$ [24]
Layer thickness, d ( $\mu\text{m}$ )	Variable	0.2	0.1	0.3	0.1	0.1
Bandgap energy, $E_g$ (eV)	3.1	2.37	3.2	3.5	3.47	3.6
Electron affinity (eV)	2.1	3.9	3.9	4	4.3	4
Dielectric permittivity, $\epsilon$ (relative)	6.5	30	9	9	9	9
Effective density of conduction band, $N_C$ ( $\text{cm}^{-3}$ )	$2.5 \times 10^{19}$	$2.4 \times 10^{20}$	$1 \times 10^{19}$	$9.2 \times 10^{18}$	$2 \times 10^{18}$	$2.2 \times 10^{18}$
Effective density of valence band, $N_V$ ( $\text{cm}^{-3}$ )	$2.5 \times 10^{19}$	$2.5 \times 10^{20}$	$1 \times 10^{19}$	$1.8 \times 10^{19}$	$1.8 \times 10^{20}$	$1.8 \times 10^{19}$
Thermal velocity of electrons, $V_e$ (cm/s)	$1 \times 10^7$	$1 \times 10^7$	$1 \times 10^7$	$1 \times 10^7$	$1 \times 10^7$	$1 \times 10^7$
Thermal velocity of holes, $V_h$ (cm/s)	$1 \times 10^7$	$1 \times 10^7$	$1 \times 10^7$	$1 \times 10^7$	$1 \times 10^7$	$1 \times 10^7$
Electron mobility, $\mu_e$ ( $\text{cm}^2/\text{Vs}$ )	100	5	20	20	100	100
Hole mobility, $\mu_h$ ( $\text{cm}^2/\text{Vs}$ )	43.9	5	10	10	25	25
Density of donors, $N_D$ ( $\text{cm}^{-3}$ )	NA	NA	$1 \times 10^{16}$	$1 \times 10^{19}$	$1 \times 10^{19}$	$1 \times 10^{17}$
Density of acceptors, $N_A$ ( $\text{cm}^{-3}$ )	$1 \times 10^{18}$	$1 \times 10^{17}$	NA	NA	NA	NA

### 3. Results and Discussion

#### 3.1. The Analysis of CuI Layer Thickness

Thickness in HTL material play a key role in producing the PCE. Thicker HTL layer may led to a higher chance of recombination to occur due to the longer travel distance of charges for the diffusion process. This condition in turn causes a decrease in the efficiency of the device [25]. Due to this circumstance, the maximum efficiency of SSDSSC is achieved at the optimum thickness of CuI and the trend in which the efficiency decreases are also determined.

Figure 3 shows that an increase in the CuI layer thickness of less than 2  $\mu\text{m}$  resulted in a drastic increase in DSSC efficiency for both devices with and without back contact. As the thickness of CuI increases, more photons can be absorbed into the cell and hence creating more electron-and-hole pairs in a depletion region [25]. These will produce an excess of carrier concentration and generate higher  $J_{sc}$  that leads to the high efficiency of SSDSSC. Moreover, at low thicknesses, the possibility of incomplete CuI layer formation can occur and cause the bonds between atoms to weaken.

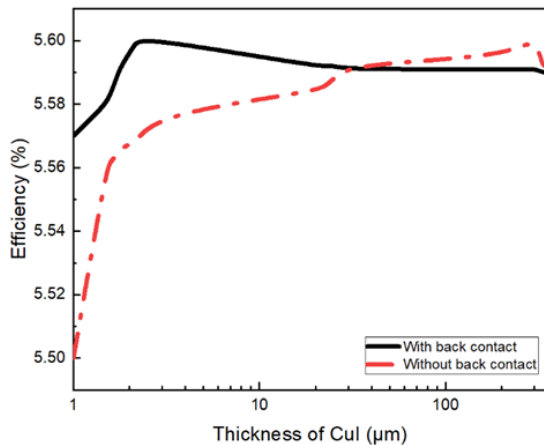


Fig. 3. The optimum thickness CuI thickness of device with and without the presence of Ni as a back contact on the efficiency of SSDSSC.

As a result, SSDSSCs have achieved similar value of cell efficiency of 5.6% for both with and without back contact devices, but at a different thickness of 2.2  $\mu\text{m}$  and 310.1  $\mu\text{m}$  respectively. Since the thickness of HTL layer above 100  $\mu\text{m}$  is considered thick, and thus increases the cost of the device. The SSDSSC with Ni back contact is preferred as a complete solar cell device.

#### 3.2 The Analysis of Doping Density $N_A$

In this work, the doping acceptor density of CuI was varied at a range between  $1 \times 10^{10} \text{ cm}^{-3}$  to  $1 \times 10^{22} \text{ cm}^{-3}$ . Based on Fig. 4, the efficiency of solar cells increases along with the increase of doping acceptor density of CuI. Such an rises causes the surface and layer

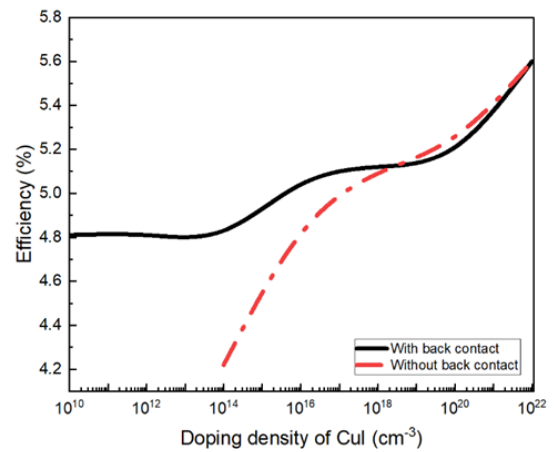


Fig. 4. The variation of CuI doping acceptor density with and without the presence of Ni as a back contact on the efficiency of SSDSSC.

resistance of HTL to decline, and thus enhanced the current flow of the cell. However, doping concentration continues to surge to a certain extent, then, due to heavy doping, the Moss-Burstein effect occurs. This will eventually hamper the performance of solar cells due to extra recombination center is created [23, 26].

Recombination rate analysis was also performed to further investigates the influence of doping acceptor density on the performance of SSDSSC. Fig. 5 and Fig. 6 show that the recombination rate occurred mainly at the absorbent layer of N719 dye at a distance between 2.2  $\mu\text{m}$  to 2.4  $\mu\text{m}$  and 310.1  $\mu\text{m}$  to 310.3  $\mu\text{m}$  for with and without back contact devices respectively. Both devices show a similar trend that at higher doping densities, the recombination rate is lower and thus, results in higher SSDSSC efficiency. This is most probably due to fewer number of random electrons that are not generating current, then will recombine with holes adjacent to the front and back contact surface. Hence, fewer holes that could be used for current generating are carried away by the random electrons [27, 28].

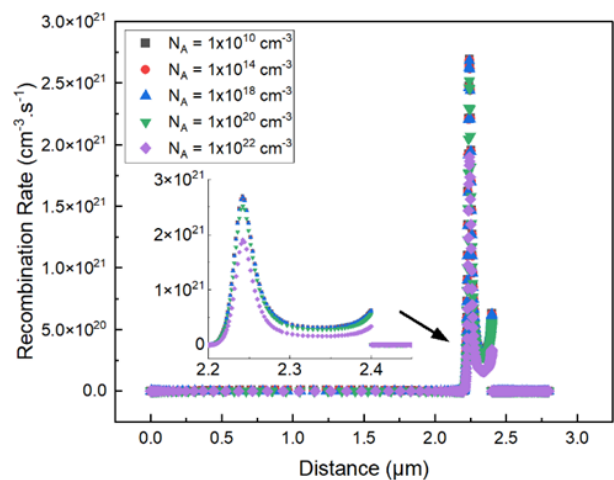


Fig. 5. The recombination rate of SSDSSC with back contact based on the variation of doping acceptor density.

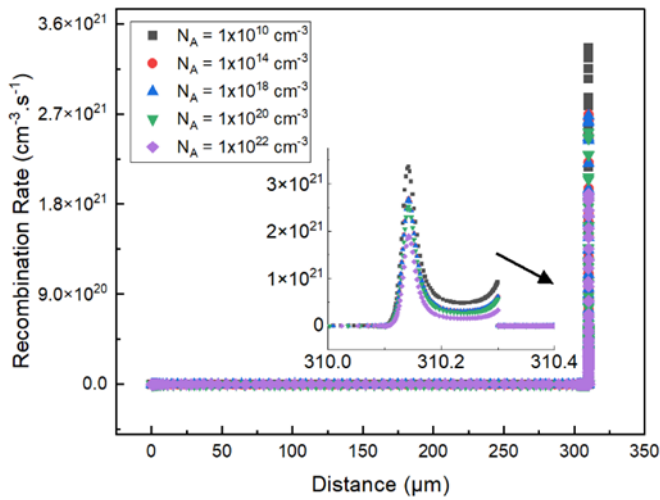


Fig. 6. The recombination rate of SSDSSC without back contact based on the variation of doping acceptor density.

### 3.2. The Analysis of Working Temperature

With significant temperature differences between locations allows solar cell performance analysis to be important and relevant. Here, the temperature was varied at a range between 280 K to 360 K. Based on Fig. 7, it can be observed that as the working temperature increase, the efficiency of the solar cell decreases with a declination trend of approximately  $-0.01\%$  per Kelvin for both with and without back contact. Compared to conventional silicon solar cells where the downward trend is in the range between  $-0.02\%$  to  $-0.03\%$  per Kelvin, shows that this work is stable and can withstand in harsh environments, yet its efficiency is less than  $10\%$ . The decrease in efficiency with temperature in solar cell device is mainly due to the high absorption of energy by the electrons at high temperatures. The electron are excited to move to an unstable state and cause the recombination before reaching the conduction band [29, 30].

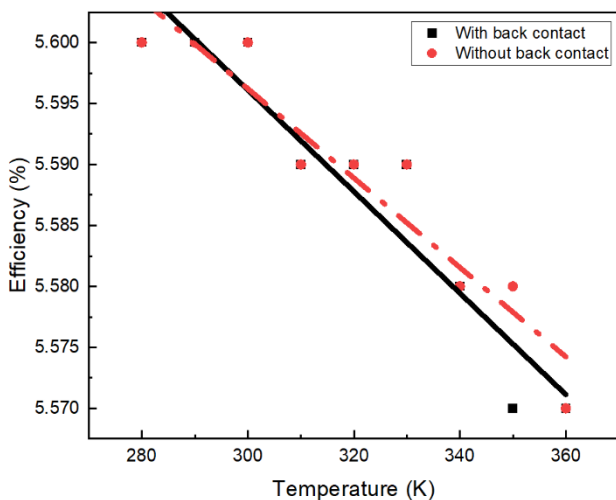


Fig. 7. The variation of working temperature with and without the presence of Ni as a back contact on the efficiency of SSDSSC.

### 3.3. The Analysis of Different Back Contact Materials

The presence of a back contact has a great influence on the performance of SSDSSC. Various types of back contacts were employed to analyze the performance of SSDSSC utilizing CuI as HTL. Ni and Pt achieved the highest efficiency among other back contacts of  $5.6\%$  as shown in Fig. 8. As the metal work function of the back contact increase, the efficiency of SSDSSC also increase. At a high metal work function, the majority carrier barrier height is decrease due to the band bending at the metal-semiconductor interface and hence, the contact becomes more ohmic [31]. Although both Ni and Pt have the highest efficiency, Ni is preferred due to its abundant material and also non-toxic substance [32].

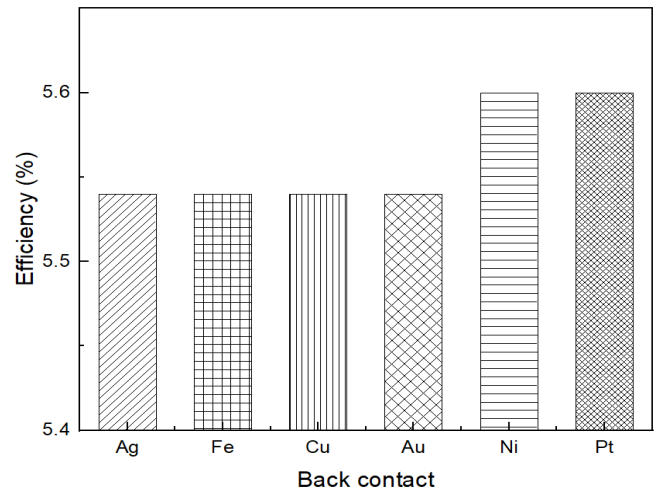


Fig. 8. The variation of back contact material on the efficiency of SSDSSC.

### 3.4. The Analysis of Defect Density at CuI/N719 and N719/TiO<sub>2</sub> Interface

The effect of defect density at interlayer of CuI/N719 and N719/TiO<sub>2</sub> were also investigated. It is inevitable that the defects exist in the bulk and at interface of each layer within the solar cell device. It has a huge influence on the performance of the device. The defects found in the form of point defects such as interstitial, lattice excess or vacancy, Schottky and Frenkel defects etc. Apart from that, the higher order defects like dislocations and grain boundaries may also be present.

At lower interface defect densities, cell efficiency was unaffected, for both the CuI/N719 and N719/TiO<sub>2</sub> interface layers as shown in Fig. 9. However, cell efficiency began to decrease dramatically at interface defect densities of  $1 \times 10^8 \text{ cm}^{-2}$  and  $1 \times 10^{14} \text{ cm}^{-2}$  for the CuI/N719 and N719/TiO<sub>2</sub> interface layers, respectively. This is due to the deteriorating quality in the layers and the increased recombination rate which causes more traps to be present at the interface [23]. These findings

indicate that the CuI/N719 interface is easily affected, and a high level of attention must be emphasized with strict quality control to ensure that cell performance is not disrupted.

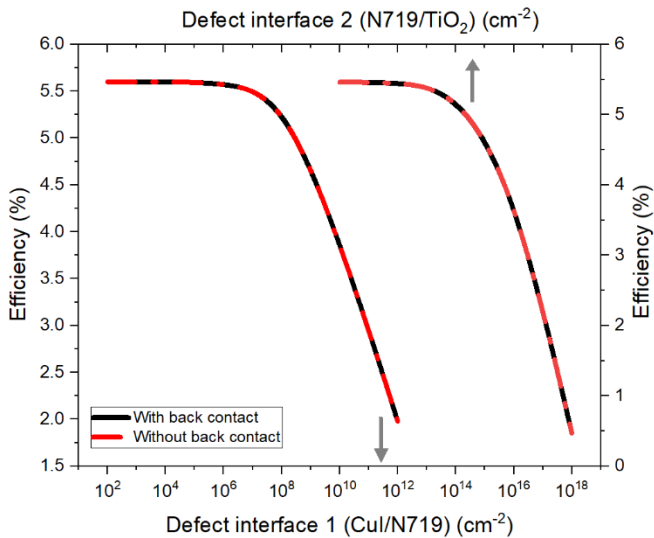


Fig. 9 The variation of defect interface 1 and 2 with and without the presence of Ni as a back contact on the efficiency of SSDSSC.

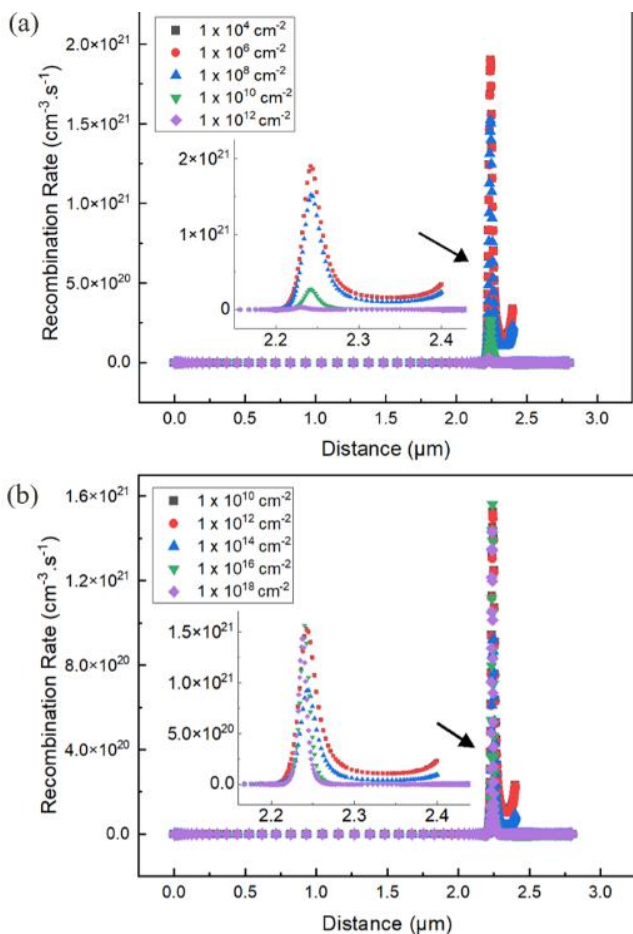


Fig. 10. The recombination rate of SSDSSC on the variation at interface defect at CuI/N719 (above) and at N719/TiO<sub>2</sub> (bottom).

Recombination rate analysis was also performed to further investigate the influence of defects at CuI/N719 and N719/TiO<sub>2</sub> interfaces. Device was simulated with 2.2 μm thick CuI layer and incorporated with Ni back contact. Figure 10 shows that the rate recombination vary at various interface defect densities for both sites. The recombination rate is appearing to be dominant at the absorbent layer of N719 dye, 2.3 μm from the front contact for both interface defect analysis sites. Rate recombination were observed to peak up to  $2 \times 10^{21} \text{ cm}^{-3} \cdot \text{s}^{-1}$  and  $1.5 \times 10^{21} \text{ cm}^{-3} \cdot \text{s}^{-1}$  for CuI/N719 and N719/TiO<sub>2</sub> interfaces respectively. This indicates that the former site is more impactful, in line with the analysis obtained in Fig. 9. However, the recombination rate increased with a decreases of defect density at both interface CuI/N719 and interface N719/TiO<sub>2</sub> layer. As the recombination centers are formed, several photo-generated carriers are trapped before they can reach the solar cell terminal. As a result, the free carrier lifetime is reduced and thus interfere the current flow [29].

### 3.5. The Analysis of Different ETL Material, Absorbent Layer

Both SSDSSC with and without back contact yielded a similar PCE of 5.6%, but device with Ni back contact is favored as it requires a lower layer thickness of 2.2 μm. The thinner layer results in less material consumption and thus lowers production costs. Moreover, the back contact of Ni is able to reflect back the unabsorbed light and maximize the absorption of light into the cell and in turn increase the value of PCE [1, 4].

To further enhance the SSDSSC, several different ETL material such as TiO<sub>2</sub>, ZnO, and SnO<sub>2</sub> was also analysed. Layer thickness for all ETL material was set at 0.2 μm. Simulated results show that among all the ETL materials in SSDSSC, TiO<sub>2</sub> yields the highest cell efficiency of 5.6%. Meanwhile, other ETL materials showed relatively less promising performance by producing cell efficiencies of 5.57% and 5.55% for ZnO and SnO<sub>2</sub> respectively. In addition, the TiO<sub>2</sub> material possess promising characteristics; a wider bandgap, abundant material, low cost, high stability and are amenable to low temperature, attain to be the best option for ETL in SSDSS [33–35].

In addition, other absorbent materials were also studied in the device structure. The conventional dye of N719 was replaced with CH<sub>3</sub>NH<sub>3</sub>PbI<sub>3</sub> and CH<sub>3</sub>NH<sub>3</sub>SnI<sub>3</sub>. Table 2 depicted the parameters of the absorbent layer in device modeling of SSDSSC. Both materials are classified as perovskite and have recently gained attention as vital materials in Perovskite Solar Cell (PSC). Absorbent layer of CH<sub>3</sub>NH<sub>3</sub>SnI<sub>3</sub> absorbed more sunlight and thus yielded the best cell efficiency as high as 29.84% as shown in Fig. 11. Meanwhile, CH<sub>3</sub>NH<sub>3</sub>PbI<sub>3</sub> produced an efficiency of 24.93% compared than that of N719 dye, with merely 5.6%. These findings are supported by the quantum efficiency analysis. Figure 12 revealed that the absorbent layer of CH<sub>3</sub>NH<sub>3</sub>SnI<sub>3</sub> absorbed wider range of sunlight

wavelength, from 300 nm up to 900 nm with maximum absorbance quantum percentage. In contrast, the N719 dye showed poor quantum efficiency performance with absorption of sunlight at short range of wavelengths. The N719 dye hardly functions as an absorbent at

wavelengths exceeding 540 nm. Therefore, the  $\text{CH}_3\text{NH}_3\text{SnI}_3$  layer is a potential absorbent layer for use in the third generation of solar cells due to it is highly efficient, Pb-free, and inexpensive [23, 32].

Table 2. Parameters of the absorbent layer in device modelling of SSDSSC.

Parameter	$\text{CH}_3\text{NH}_3\text{PbI}_3$ [23]	$\text{CH}_3\text{NH}_3\text{SnI}_3$ [23]
Layer thickness, $d$ ( $\mu\text{m}$ )	1	1
Bandgap energy, $E_g$ (eV)	1.55	1.3
Electron affinity (eV)	3.9	4.2
Dielectric permittivity, $\epsilon$ (relative)	18	10
Effective density of conduction band, $N_C$ ( $\text{cm}^{-3}$ )	$2.2 \times 10^{18}$	$1 \times 10^{18}$
Effective density of valence band, $N_V$ ( $\text{cm}^{-3}$ )	$1.9 \times 10^{19}$	$1 \times 10^{18}$
Thermal velocity of electrons, $V_e$ (cm/s)	$1 \times 10^7$	$1 \times 10^7$
Thermal velocity of holes, $V_h$ (cm/s)	$1 \times 10^7$	$1 \times 10^7$
Electron mobility, $\mu_e$ ( $\text{cm}^2/\text{Vs}$ )	3	1.6
Hole mobility, $\mu_h$ ( $\text{cm}^2/\text{Vs}$ )	17	1.6
Density of donors, $N_D$ ( $\text{cm}^{-3}$ )	NA	NA
Density of acceptors, $N_A$ ( $\text{cm}^{-3}$ )	$1 \times 10^{13}$	$3.2 \times 10^{15}$

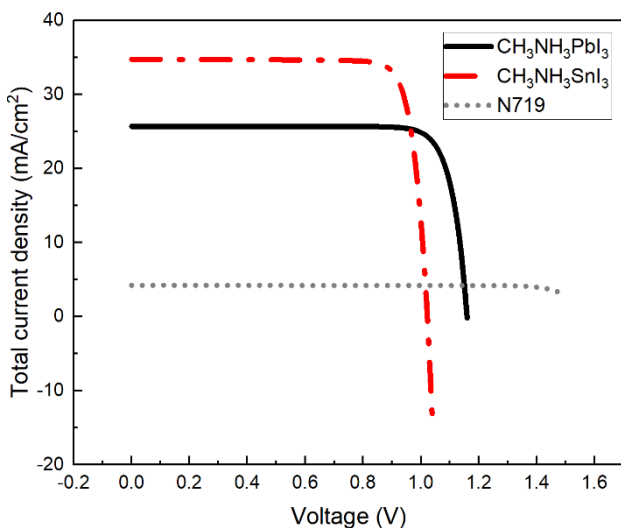


Fig. 11. A J-V curve for the variation of absorbent layer for SSDSSC with back contact.

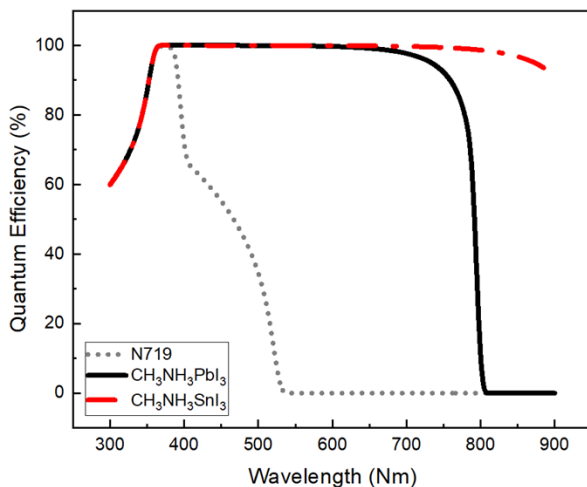


Fig. 12. The quantum efficiency for the variation of absorbent layer for SSDSSC with back contact.

### 3.6. The Analysis of Dark and Light Illumination

Solar cell can function under both illumination condition, dark and light illuminations. Figure 13 illustrates the dark current retained at zero current from negative voltage to 1.2 V, indicating no leakage current in the reverse bias. Hence, the simulated device able to operate accurately. Furthermore, the rate recombination tends to occur at absorbent layer,  $2.35 \mu\text{m}$  from the front contact at higher rate of  $7.7 \times 10^{21} \text{ cm}^{-3} \cdot \text{s}^{-1}$  compared to light condition as shown in Fig. 14. Noted that the light illumination is identical Fig. 10(a) and is included here for comparison. Figure 14 shows a normal phenomenon that occurs in a solar cell where the I-V curve of light illuminated is the dark I-V curve that is being shifted by the light-generated current. For both cases, the current is identical [4, 33].

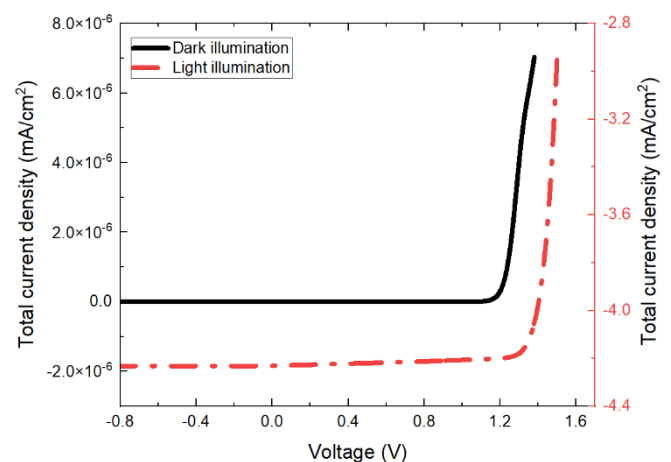


Fig. 13. A J-V curve of the performance of SSDSSC with back contact under dark and light illumination.

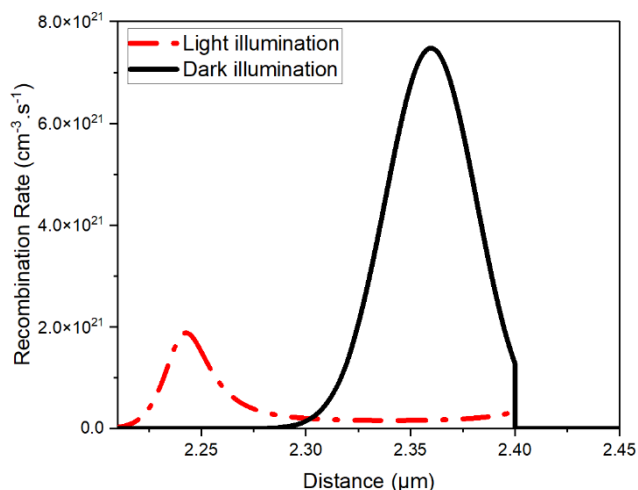


Fig. 14. A recombination rate of SSDSSC with back contact under dark and light illumination.

#### 4. Conclusion

Herein, the optimal key parameters with CuI as HTL in SSDSSC have been obtained. The value of PCE is not very encouraging but has confirmed that with in-depth analysis, cell efficiency can be improved. By replacing the N719 dye with  $\text{CH}_3\text{NH}_3\text{SnI}_3$  perovskite material, the performance of the device is further elevated. Although the back contact seems insignificant, it also plays a major role in the structure of solar cells. The selection of  $\text{TiO}_2$  as the ETL has been encouraging in maintaining the performance of the device. Overall, the cell efficiency of the simulated SSDSSC has been effectively increased by employing the appropriate back contact, at optimized parameters as well as controlling the defect density to a certain level. This work thereby provides a clear insight to be employed as a parameter guidance in fabricating SSDSSC.

#### Acknowledgment

This work was supported by Universiti Teknikal Malaysia Melaka and Ministry of Education Malaysia under RACER/2019/FKEKK-CETRI/F00403

#### References

- [1] S. Sharma, K. K. Jain, and A. Sharma, "Solar cells: In research and applications," *Mater. Sci. Appl.*, vol. 6, no. 12, pp.1145–1155, 2015.
- [2] H. N. Wunn, S. Motoda, M. Morita, and S. Katayose, "Improvement in photocatalytic effects of dye sensitized titanium dioxide by hydroxyapatite coating," *Engineering Journal*, vol. 24, no. 4, pp. 63–71, 2020.
- [3] W. Waluyo, S. Syahrial, and F. Yasin, "Design and investigation of miniature solar cell source inductive wireless power transfer on various distances, turns and loads," *Engineering Journal*, vol. 22, no. 4, pp. 121–145, 2018.
- [4] M. Green, *Solar Cells: Operating Principles, Technology and System Applications*. Englewood Cliffs, 1981.
- [5] N. S. Noorasid, F. Arith, A. N. Mustafa, S. Mahalingam, P. Chelvanathan, and N. Amin, "Current advancement of flexible dye sensitized solar cell: A review," *Optik (Stuttg)*, vol. 254, p. 168089, 2022.
- [6] I. Bhattacharya, S. Chakrabarti, H. S. Reehal, and V. Lakshminarayanan, *Advances in Optical Science and Engineering: Proceedings of the Third International Conference*. Springer Singapore, 2017.
- [7] N. S. Noorasid, F. Arith, S. N. Alias, A. N. Mustafa, H. Roslan, S. H. Johari, H. R. A. Rahim, and M. M. Ismail, "Synthesis of ZnO nanorod using hydrothermal technique for dye-sensitized solar cell application," in *Intell. Manuf. Mechatronics*. Singapore: Springer, 2021, pp. 895–905.
- [8] D. N. Liyanage, K. D. M. S. P. K. Kumarasinghe, G. R. A. Kumara, A. C. A. Jayasundera, K. Tennakone, and B. Onwona-Agyeman, "Donor- $\pi$ -conjugated spacer-acceptor dye-sensitized solid-state solar cell using cui as the hole collector," *Int. J. Photoenergy*, vol. 2019, 2019, Art. no. 1653027.
- [9] F. Jahantigh and M. J. Safikhani, "The effect of HTM on the performance of solid-state dye-sensitized solar cells (SDSSCs): A SCAPS-1D simulation study," *Appl. Phys. A Mater. Sci. Process*, vol. 125, no. 4, pp. 1–7, 2019.
- [10] P. P. Zhang, Z. J. Zhou, D. X. Kou, and S. X. Wu, "Perovskite thin film solar cells based on inorganic hole conducting materials," *Int. J. Photoenergy*, vol. 2017, 2017, Art. no. 6109092.
- [11] M. A. Azhari, F. Arith, F. Ali, S. Rodzi, and K. Karim, "Fabrication of low cost sensitized solar cell using natural plant pigment dyes," *ARPN J. Eng. Appl. Sci.*, vol. 10, no. 16, pp. 7092-7096, 2015.
- [12] D. K. Kaushik, M. Selvaraj, S. Ramu, and A. Subrahmanyam, "Thermal evaporated Copper Iodide (CuI) thin films: A note on the disorder evaluated through the temperature dependent electrical properties," *Sol. Energy Mater. Sol. Cells.*, vol. 165, pp. 52–58, 2017.
- [13] M. N. Amalina, Y. Azilawati, N. A. Rasheid, and M. Rusop, "The properties of copper (I) iodide (CuI) thin films prepared by mister atomizer at different doping concentration," *Procedia Eng.*, vol. 56, pp. 731–736, 2013.
- [14] A. Tricoli, A. S. Wallerand, and M. Righettoni, "Highly porous  $\text{TiO}_2$  films for dye sensitized solar cells," *J. Mater. Chem.*, vol. 22, pp. 14254–14261, 2012.
- [15] F. Arith, S. A. M. Anis, M. M. Said, and C. M. I. Idris, "Low cost electro-deposition of cuprous oxide P-N homo-junction solar cell," *Adv. Mater. Res.*, vol. 827, pp. 38–43, 2014.
- [16] E. C. Smith and D. Venkataraman, "Deleterious Effects of Halides and Solvents on the Integrity of Copper Iodide Hole Extraction Layers in Hybrid Perovskite Photovoltaics," 2021, doi: 10.26434/chemrxiv-2021-4nmd7.

- [17] P. Singh, A. Raman, and N. Kumar, "Spectroscopic and simulation analysis of facile PEDOT:PSS layer deposition-silicon for perovskite solar cell," *Silicon*, vol. 12, pp. 1769–1777, 2020.
- [18] J. Song, X. Yin, L. Hu, Z. Su, Y. Jin, D. Deng, Z. Li, G. Wang, Q. Bao, and W. Tian, "Plasmon-coupled Au-nanochain functionalized PEDOT:PSS for efficient mixed tin-lead iodide perovskite solar cells," *Chem. Commun.*, vol. 58, pp. 1366-1369, 2022.
- [19] G. Yongjin, B. Xueguang, L. Yucheng, Q. Binyi, L. Qingliu, and J. Qubo, "Numerical investigation energy conversion performance of tin-based perovskite solar cells using cell capacitance simulator," *Energy*, vol. 13, no. 22, p. 5907, 2020.
- [20] M. Kemerink, S. Timpanaro, M. de Kok, E. Meulenkamp, and F. Touwslager, "Three-dimensional inhomogeneities in PEDOT:PSS films," *J. Phys. Chem. B.*, vol. 108, pp. 18820–18825, 2004.
- [21] K. S. Nithya and K. S. Sudheer, "Device modelling of non-fullerene organic solar cell with inorganic CuI hole transport layer using SCAPS 1-D," *Optik (Stuttg.)*, vol. 217, p. 164790, 2020.
- [22] M. Burgelman, K. Decock, A. Niemegeers, J. Verschraegen, and S. Degraeve, *SCAPS Manual*. 2020.
- [23] F. Anwar, R. Mahbub, S. S. Satter, and S. M. Ullah, "Effect of different HTM layers and electrical parameters on ZnO nanorod-based lead-free perovskite solar cell for high-efficiency performance," *Int. J. Photoenergy*, vol. 2017, 2017, Art no. 9846310.
- [24] V. Shukla and G. Panda, "The performance study of CdTe/CdS/SnO<sub>2</sub> solar cell," *Mater. Today Proc.*, vol. 26, pp. 487–491, 2019.
- [25] U. Mandadapu, S. V. Vedanayakam, and K. Thyagarajan, "Simulation and analysis of lead based perovskite solar cell using SCAPS-1D," *Indian J. Sci. Technol.*, vol. 10, pp. 1–8, 2017.
- [26] P. Chelvanathan, S. A. Shahahmadi, F. Arith, K. Sobayel, M. Aktharuzzaman, A. K. Sopian, F. H. Alharbi, and N. Tabet, "Effects of RF magnetron sputtering deposition process parameters on the properties of molybdenum thin films," *Thin Solid Films*, vol. 638, pp. 213–219, 2017.
- [27] M. Atowar Rahman, "Enhancing the photovoltaic performance of Cd-free Cu<sub>2</sub>ZnSnS<sub>4</sub> heterojunction solar cells using SnS HTL and TiO<sub>2</sub> ETL," *Sol. Energy*, vol. 215, pp. 64–76, 2021.
- [28] S. Abdelaziz, A. Zekry, A. Shaker, and M. Abouelatta, "Investigating the performance of formamidinium tin-based perovskite solar cell by SCAPS device simulation," *Opt. Mater. (Amst.)*, vol. 101, p. 109738, 2020.
- [29] P. K. Patel, "Device simulation of highly efficient eco-friendly CH<sub>3</sub>NH<sub>3</sub>SnI<sub>3</sub> perovskite solar cell," *Sci. Rep.*, vol. 11, pp. 1–11, 2021.
- [30] O. V. Aliyaselvam, F. Arith, A. N. Mustafa, M. K. Nor, and O. Al-Ani, "Solution processed of solid state HTL of CuSCN layer at low annealing temperature for emerging solar cell," *Int. J. Renew. Energy Res.*, vol. 11, no. 2, p. 10, 2021.
- [31] F. Behrouznejad, S. Shahbazi, N. Taghavinia, H. P. Wu, and E. Wei-Guang Diao, "A study on utilizing different metals as the back contact of CH<sub>3</sub>NH<sub>3</sub>PbI<sub>3</sub> perovskite solar cells," *J. Mater. Chem. A.*, vol. 4, pp. 13488–13498, 2016.
- [32] M. Asyadi Azam, N. Ezyanie Safie, M. Fareezuan Abdul Aziz, R. Noor Amalina Raja Seman, M. Rafi Suhaili, A. Abdul Latiff, F. Arith, A. Mohamed Kassim, and M. Hanafi Ani, "Structural characterization and electrochemical performance of nitrogen doped graphene supercapacitor electrode fabricated by hydrothermal method," *Int. J. Nanoelectron. Mater.*, vol. 14, pp. 127–136, 2021.
- [33] A. Husainat, W. Ali, P. Cofie, J. Attia, J. Fuller, and A. Darwish, "Simulation and analysis method of different back metals contact of CH<sub>3</sub>NH<sub>3</sub>PbI<sub>3</sub> perovskite solar cell along with electron transport layer TiO<sub>2</sub> using MBMT-MAPLE/PLD," *Am. J. Opt. Photonics.*, vol. 8, no. 1, p. 6, 2020.
- [34] S. H. Meriam Suhaimy, N. Ghazali, F. Arith, and B. Fauzi, "Enhanced simazine herbicide degradation by optimized fluoride concentrations in TiO<sub>2</sub> nanotubes growth," *Optik (Stuttg.)*, vol. 212, p. 164651, 2020.
- [35] N. S. Noorasid, F. Arith, A. N. Mustafa, M. A. Azam, S. H. Meriam Suhaimy, and O. A. Al-ani, "Effect of low temperature annealing on anatase TiO<sub>2</sub> layer as photoanode for dye-sensitized solar cell," *Przegląd Elektrotechniczny*, vol. 97, pp. 12–16, 2021.
- [36] A. Nizamuddin, F. Arith, I. J. Rong, M. Zaimi, A. S. Rahimi, and S. Saat, "Investigation of copper(I)thiocyanate (CuSCN) as a hole transporting layer for perovskite solar cells application," *J. Adv. Res. Fluid Mech. Therm. Sci.*, vol. 78, pp. 153–159, 2021.
- [37] M. Green, *Power to the People: Sunlight to Electricity Using Solar Cells*. UNSW Press, 2000.
- [38] W. Y. Chen, L. L. Deng, S. M. Dai, X. Wang, C. B. Tian, X. X. Zhan, S. Y. Xie, R. Bin Huang, and L. S. Zheng, "Low-cost solution-processed copper iodide as an alternative to PEDOT:PSS hole transport layer for efficient and stable inverted planar heterojunction perovskite solar cells," *J. Mater. Chem. A.*, vol. 3, pp. 19353–19359, 2015.
- [39] Z. Cai, S. Chen, "Extrinsic dopants in quasi-one-dimensional photovoltaic semiconductor Sb<sub>2</sub>S<sub>3</sub>: A first-principles study," *J. Appl. Phys.*, vol. 127, p. 183101, 2020.
- [40] C. Du, X. Wang, W. Chen, S. Feng, J. Wen, and Y. A. Wu, "CO<sub>2</sub> transformation to multicarbon products by photocatalysis and electrocatalysis," *Mater. Today Adv.*, vol. 6, p. 100071, 2020.



**Nur Syamimi Noorasid**, photograph and biography not available at the time of publication.



**Faiz Arith** received the B. Eng. in Electrical & Electronic Engineering from University of Fukui, Japan, in 2010. Then he obtained M.Sc in Microelectronic from National University of Malaysia in 2012 and the Ph.D. degree in Semiconductor Devices from Newcastle University, United Kingdom, in 2018.

Currently, he is Senior Lecturer and the Head of Micro and Nano Electronic Research Group in Universiti Teknikal Malaysia, Melaka, Malaysia. He is the author of two book chapters, more than 30 articles, and has won several innovation competitions. His main research interest is fabrication and simulation of semiconductor devices including solar cells, MOSFETs, power semiconductor devices and optoelectronic devices. He is a Technical Editor of the Journal of Telecommunication, Electronic and Computer Engineering, and has served as reviewer in more than 20 indexed reputable journals.

**Ain Yasmin Firhat**, photograph and biography not available at the time of publication.

**Ahmad Nizamuddin Mustafa**, photograph and biography not available at the time of publication.

**Ahmad Syahiman Mohd Shah**, photograph and biography not available at the time of publication.